Desalination and Water Treatment
www.deswater.com

doi: 10.1080/19443994.2015.1079261

57 (2016) 15533–15546
July

Taylor & Francis
Taylor & Francis Group

Study on the mechanism of cerium oxide catalytic ozonation for controlling the formation of bromate in drinking water

Qun Wang[a,*], Zhichao Yang[a], Jun Ma[b], Jiangchuan Wang[a], Lin Wang[a], Mingkun Guo[a]

[a]*Faculty of Geosciences and Environmental Engineering, Southwest Jiaotong University, Chengdu 610031, P.R. China, Tel. +86 18215559048; email: zcyang_swjtu@126.com (Q. Wang), Tel. +86 13654560552; email: yzc096015@163.com (Z. Yang), Tel. +86 13699438483; email: 360263618@qq.com (J. Wang), Tel. +86 15982096046; email: 519403524@qq.com (L. Wang), Tel. +86 13709070813; email: 1349609740@qq.com (M. Guo)*

[b]*School of Municipal and Environmental Engineering, Harbin Institute of Technology, Harbin 150090, P.R. China, Tel. +86 451 86283010; email: majunhit@126.com*

Received 31 March 2015; Accepted 10 July 2015

ABSTRACT

This study evaluated the formation of bromate (BrO_3^-) in the catalytic ozonation with cerium oxide (CeO_2) compared with single ozonation and several catalytic ozonation with metal oxides (i.e. magnesium oxide (MgO) and synthetic goethite (FeOOH)). The results showed that the least BrO_3^- was generated in the O_3/CeO_2 system. Primary experiments have confirmed that both Br^- and BrO_3^- could be hardly adsorbed by CeO_2, and thus the inhibition of BrO_3^- in the O_3/CeO_2 process was mainly ascribed to the effect of CeO_2 on the ozone decomposition and subsequent hydroxyl radical ($HO^{\bullet}$) formation in the bulk solution. Firstly, the degradation of para-chloronitrobenzene (pCNB) was examined and the results showed that less pCNB was degraded by O_3/CeO_2 than single ozonation, suggesting that $HO^{\bullet}$ formation was inhibited in the O_3/CeO_2 system. Furthermore, the effect of inorganic anions (i.e. sulfate (SO_4^{2-}) and nitrate (NO_3^-)) on the systems was investigated. It was found that SO_4^{2-} had a negative effect on the BrO_3^- inhibition in the O_3/CeO_2 process, which was due to that SO_4^{2-} inhibited the adsorption of O_3 and oxygen-containing species by CeO_2 through competing the active sites of CeO_2. Moreover, the inhibition of BrO_3^- formation in the catalytic ozonation with the CeO_2 samples calcined at different temperatures was also studied. The results showed that the efficiency of inhibition decreased in the following sequence CeO_2 (450°C) > CeO_2 (650°C) > CeO_2 (250°C). X-ray diffraction (XRD) and X-ray photoelectron spectroscopy (XPS) analyses on the CeO_2 specimens showed that CeO_2 (450°C) had the highest Ce(IV) to Ce(III) ratio and the least lattice oxygen and adsorbed oxygen amount. Therefore, a new mechanism about the inhibition of BrO_3^- formation in the O_3/CeO_2 system was proposed. Both O_3 molecules and some oxygen-containing intermediates from O_3 decomposition in solution will be adsorbed on the active sites of CeO_2, and the less lattice and adsorbed oxygen also promote the adsorption of oxygen-containing species on the CeO_2 surface. This will result in the inhibition of O_3 decomposition into $HO^{\bullet}$ in solution and thus inhibition of BrO_3^- formation. This study improves our understanding of the O_3/CeO_2 process for controlling BrO_3^- formation and also guides the practical application.

*Corresponding author.

Keywords: Cerium dioxide; Ozonation; Bromate; Sulfate; Calcination

1. Introduction

Ozone is widely used in water treatment processes to efficiently oxidize organic pollutants containing aromatic rings, amino groups, or conjugated double bonds [1]. However, single ozonation seems to be powerless to remove the emerged refractory contaminants (e.g. endocrine disrupting chemicals, pharmaceuticals, and pesticides) due to its low reactivity and high selectivity, and thus considerable effort has been centered on heterogeneous catalytic ozonation with metal oxides in recent years [2,3].

Heterogeneous catalytic ozonation with metal oxides is a promising process to enhance the degradation of refractory pollutants without extra addition of chemicals and energy in water. Compared with traditional ozonation, catalytic ozonation with metal oxides can enhance ozone utilization and also improve the mineralization of various pollutants [4]. In the past decades, different mechanisms of catalytic ozonation with various metal oxides (e.g. FeOOH, MnO_2, TiO_2, Al_2O_3, TiO_2/Al_2O_3, and CuO/CeO_2) have been proposed from extensive researches. For instance, Zhang et al. [5] reported that the catalytic ozonation with synthetic goethite (FeOOH) could substantially enhance nitrobenzene decontamination compared with single ozonation via promoting hydroxyl radical ($HO^{\bullet}$) formation; Beltrán et al. [6] suggested that a conspicuous 80% of oxalic acid conversion during the TiO_2/Al_2O_3 catalytic ozonation was obtained via the reaction between adsorbed oxalic acid and ozone in solution; Rosal et al. [7] noted the inhibition of $HO^{\bullet}$ formation at a neutral pH during the degradation of naproxen and carbamazepine by TiO_2 catalytic ozonation and suggested the surface reaction between the metal–organic complexes and active groups generated from O_3 decomposition on the catalyst surface led to the mineralization of target compounds.

Additionally, bromate (BrO_3^-), an undesired byproduct formed during ozonation of bromide-containing water is also taken into consideration. Because of its carcinogenic and genotoxic property, it is regulated in drinking water at a maximum contaminant level (MCL) of 10 μg/L by the USEPA and EU [8,9]. Once BrO_3^- is formed, it is difficult to remove BrO_3^- from treated water by conventional treatment processes. In single ozonation, the BrO_3^- inhibition has been investigated extensively [10–12]. However, the investigation of the inhibition of BrO_3^- formation in catalytic ozonation with metal oxides is limited. Nie et al. [13] reported the BrO_3^- formation during MnO_x/Al_2O_3 catalytic ozonation was lower than that in single ozonation by about 77% in the presence of 2,4-dichlorophenoxyacetic acid, suggesting both BrO_3^- and hypobromous acid/hypobromite ($HOBr/OBr^-$) were reduced to Br^- by Mn^{2+}. Another research by Nie et al. [14] reported that the adsorption of BrO_3^- on the catalyst surface and the subsequent reduction of BrO_3^- by surface Fe(II) could account for the complete removal of BrO_3^- in the β-$FeOOH/Al_2O_3$ catalytic ozonation in the presence of organic compounds. Yang and co-workers [15] applied $Ce_xZr_{1-x}O_2$-mixed oxides to minimize BrO_3^- formation during catalytic ozonation of a filtered water and found about 53% BrO_3^- was reduced by $Ce_{0.75}Zr_{0.25}O_2$ catalytic ozonation via competitive reactions between Br^- and organic compounds with $HO^{\bullet}$.

Unfortunately, to the best of our knowledge, there are few studies on the BrO_3^- inhibition by CeO_2 catalytic ozonation except for the research by Zhang and co-workers. Zhang et al. [16] found that the amount of BrO_3^- formed in the presence of CeO_2 was significantly lower than single ozonation during the oxidation of bromide-containing water and confirmed that neither the surface adsorption of BrO_3^- or Br^- on CeO_2 nor the reduction of BrO_3^- to $HOBr/OBr^-$ by CeO_2 could be accounted for the BrO_3^- minimization. Moreover, the authors suggested that the minimization of BrO_3^- might be ascribed to the surface reduction of $BrO^{\cdot}$ to $HOBr/OBr^-$ and the enhanced decomposition of H_2O_2 formed during ozone decomposition. However, no further pregnant work by the authors was done to confirm the relationship between the characteristics of CeO_2 and BrO_3^- formation. To date, the role of the CeO_2 catalyst on the BrO_3^- inhibition remains unclear.

In this study, the BrO_3^- formation during single ozonation and catalytic ozonation with several metal oxides (i.e. CeO_2, MgO, and FeOOH) was tested. The degradation of para-chloronitrobenzene (pCNB) and the effect of inorganic anions (i.e. sulfate (SO_4^{2-}) and nitrate (NO_3^-)) on the BrO_3^- minimization were also investigated. Moreover, both X-ray diffraction (XRD) and X-ray photoelectron spectroscopy (XPS) analyses were employed to explore the structural and compositional differences among the calcined CeO_2 specimens to reveal the mechanism of BrO_3^- inhibition during CeO_2 catalytic ozonation.

2. Materials and methods

2.1. Apparatus and methods

All reagents obtained from Sigma-Aldrich were of analytic grade without further purification. The stock solutions were prepared using Milli-Q ultrapure water (resistivity 18.2 MΩ cm) from a Millipore system.

Batch experiments were carried out in a 1-L round belly flask equipped with a thermostat (THD-5015, Tianheng) as shown in Fig. 1. Ozone was produced by a DHX-SS-1G ozone generator (Harbin Jiujiu Electrochemical Engineering Ltd.) using dried pure oxygen as the gas source. The oxygen flow rate was 300 mL/min and the concentration of ozone in the gas phase was 0.5–5.5 mg/L, which could be flexibly controlled by adjusting the electric current of the ozone generator.

Gaseous ozone was bubbled into the reactor through a silica dispenser over the course of 15 min to stabilize the ozone concentration. The ozone-bearing water was continuously withdrawn to measure the aqueous ozone concentration by a UV–vis Spectrometer (Model 752, Shandong Gaomi Rainbow Analysis instrument Ltd) at 258 nm (molar absorbance coefficient = 3,000 M^{-1} cm^{-1}). After the steady ozone concentration (0.4–5.21 mg/L) reached, the ozone gas was shut off. Different solutions (e.g. pCNB solution (0.05 μmol) and KBr solution (13.75–22.5 μmol)) were instantly introduced into the reactor followed by the catalysts (at a dose of 0.1 g/L unless specified). The reactor was then sealed and magnetically stirred. The samples withdrawn at predetermined intervals were filtered through 0.45-μm glass fiber filters (Whatman) to remove the catalyst particles (no impact on the target compounds was seen upon testing) after the residual ozone has been quenched by 0.025 mol/L sodium sulfate (Na_2SO_3) solution. The detailed procedures for these experiments are described in Text S1 (Supporting Information).

2.2. Catalyst preparation

Cerium nitrate and magnesium nitrate were calcined in air for two hours at 450℃ in a muffle furnace to obtain CeO_2 and MgO. The samples were crushed and screened to produce particles with a diameter of 0.075–0.3 mm. The calcination temperature of the CeO_2 sample was changed during the experiments to determine the effect of the calcination temperature of the CeO_2 specimens on the BrO_3^- inhibition.

Kandori's method [17] was employed to prepare FeOOH from the precipitation reaction of the corresponding nitrate and sodium hydroxide. FeOOH powders with an average particle diameter in the range of 0.075–0.3 mm were repeatedly rinsed with distilled water until the conductivity of the water stabilized.

2.3. Analysis method

The concentrations of BrO_3^- and Br^- ions were measured using an ICS-3000 ion chromatograph (Dionex China Ltd) equipped with an AS19 ion chromatographic column. Potassium oxide (KOH) solution (30 mmol/L) was used as the mobile phase with a flow

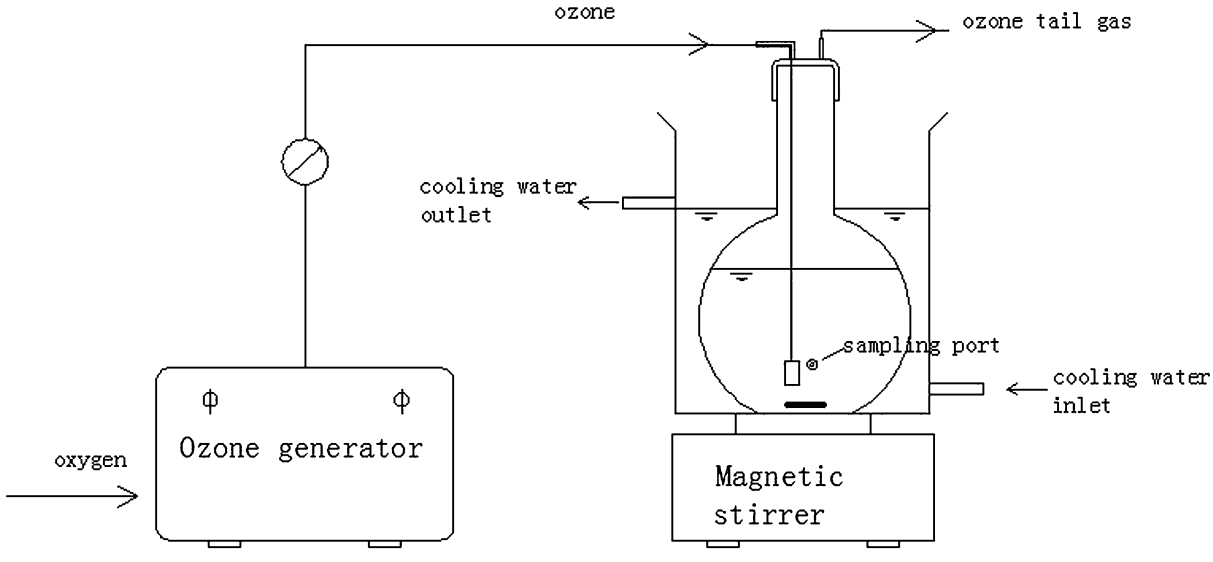

Fig. 1. Scheme of static test reactor.

rate of 1.000 mL/min. The injection volume was 100 μL. The limit of detection (LOD) and the limit of quantitation (LOQ) of the methods were calculated experimentally as a signal-to-noise ratio (S/N) of 3 and 10, respectively [18]. LOD and LOQ of Br^- determination were 2.16 and 6.29 μg/L, while in the BrO_3^- measurement, these two values were 3.55 and 9.67 μg/L, respectively. The concentration of $HOBr/OBr^-$ was determined following the method mentioned by Zhang et al. [16].

pCNB was determined on a high-performance liquid chromatography (HPLC) (Waters) equipped with a Symmetry C18 column (4.6 mm × 150 mm × 5 μm, Waters) and a UV detector at 280 nm. The eluent (1.000 mL/min) was a mixture of Milli-Q water and methanol (V:V = 30:70). The injection volume was 100 μL.

CeO_2 was characterized by XRD (D/max-2000, Rigaku) using Cu Kα radiation. The diffraction patterns of the samples were also analyzed to obtain information about the catalysts. Accordingly, the catalyst formula and the quantitative ratios of the lattice constants of each element in the crystal structure can be determined [19]. The specific surface area of the CeO_2 samples was measured using a BET surface area analyzer (ASAP 2020, Micromeritics).

Ex situ PHI-57300/ESCA X-ray photoelectron spectroscopy (XPS) was used to analyze the energy of the electron bonding of the elements on the sample surface as well as their relative content.

3. Results and discussion

3.1. Bromate formation during catalytic ozonation with different catalysts

Fig. 2(a) shows the BrO_3^- formation during ozonation and different catalytic ozonation. As shown in Fig. 2(a), the concentration of BrO_3^- formed at 30 min in the O_3/CeO_2 system (205.58 μg/L) was 56.35, 41.45, and 23.80% lower than that formed in O_3/MgO (471.01 μg/L), O_3/FeOOH (351.53 μg/L), and single ozonation (269.78 μg/L), respectively. Zhang et al. [20] reported the BrO_3^- formation was reduced by 22% during the O_3/CeO_2 process, which was in great agreement with the result obtained in the present work.

Generally, during ozonation of bromide-containing water, the formation of BrO_3^- is related to the direct ozonation and $HO^{\bullet}$ oxidation reaction [21]. The reaction scheme is shown in Fig. 3 and the main pathway of the formation of BrO_3^- is shown by the thick arrows [22,23].

The reaction rate constants and dissociation constant (pK_a) of HOBr in the scheme are obtained from Haag et al. [24] and von Gunten et al. [21,22]. As shown in Fig. 3, both HOBr and OBr^- are requisite intermediates in the BrO_3^- formation [10,21]. Thus, in the presence of CeO_2 catalyst, several possible pathways for the BrO_3^- inhibition in the O_3/CeO_2 process are considered as following: (i) the adsorption of Br^-

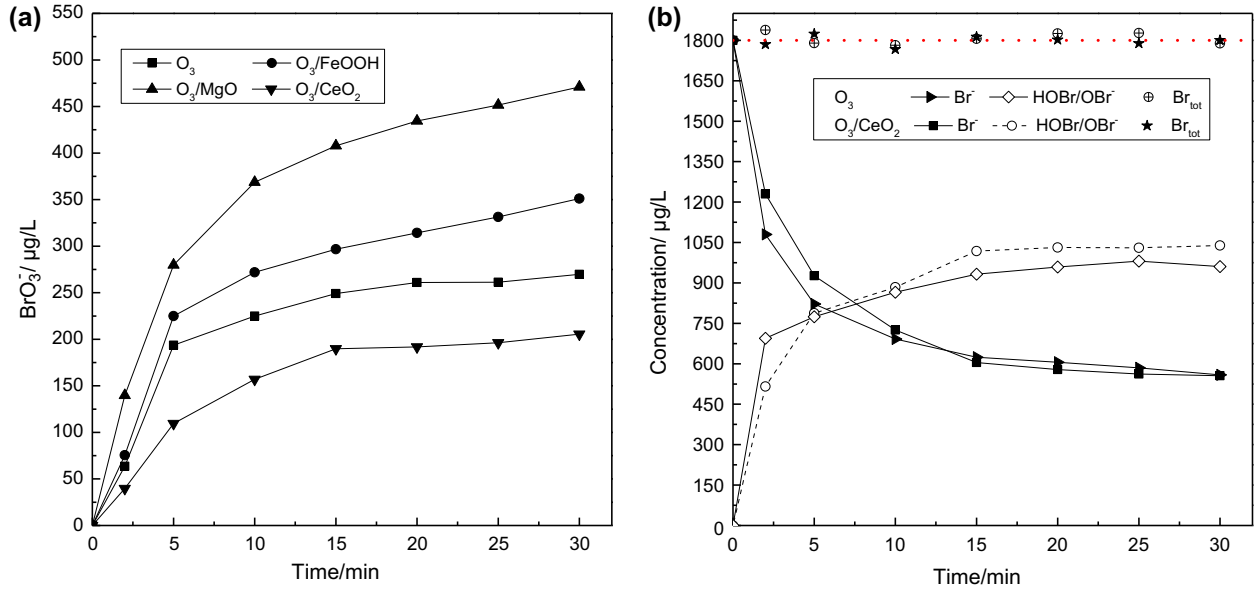

Fig. 2. (a) The bromate formation during ozonation and catalytic ozonation with different catalysts and (b) concentration profiles of Br^- and $HOBr/OBr^-$ and the corresponding total bromine mass balance during ozonation and CeO_2 catalytic ozonation. Br_{tot}: Sum of all bromine species (i.e. Br^-, HOBr, OBr^-, and BrO_3^-). $[Br^-]_0$ = 1.8 mg/L, $[O_3]_0$ = 5.21 mg/L, catalyst dose = 100 mg/L, T = 18°C, and pH 6.30.

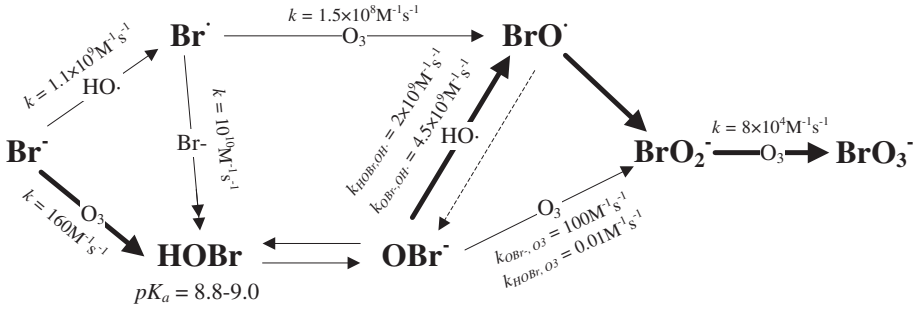

Fig. 3. The reaction scheme of the formation of BrO_3^- during ozonation. The double arrow: a three–step reaction from Br to HOBr as described by von Gunten [11].

or BrO_3^- on the CeO_2 surface; (ii) the reduction of BrO_3^- or $HOBr/OBr^-$ to Br^- by CeO_2; (iii) blocking the route from Br^- to $HOBr/OBr^-$ by CeO_2; and (iv) blocking the oxidation of $HOBr/OBr^-$ to $BrO^{\cdot}$. Under the relatively broad experimental conditions, the adsorption of Br^- or BrO_3^- on the CeO_2 surface and the reduction of BrO_3^- by CeO_2 can be ruled out according to the previous studies [13,16,20]. To verify the other possibilities, the evolution of Br species (i.e. Br^- and $HOBr/OBr^-$) and also the Br mass balance during ozonation and catalytic ozonation were investigated (Figs. 2(b), S1 and S2).

As shown in Fig. 2(b), the concentration of Br^- decreased rapidly in the first 10 min during single ozonation and the O_3/CeO_2 system, while $HOBr/OBr^-$ built up simultaneously. Slight changes of both Br^- and $HOBr/OBr^-$ occurred after 15 min as similar with BrO_3^- shown in Fig. 2(a). The behaviors could also be observed in the cases of O_3/MgO and $O_3/FeOOH$ as shown, respectively, in Figs. S1 and S2 (Supporting Information). Moreover, after 15 min, the Br^- concentrations in ozonation with and without CeO_2 were nearly the same. Combined with Figs. S1 and S2, at the end of the reactions, the concentration of residual Br^- in the processes decreased in the trend O_3 (558.7 μg/L) > O_3/CeO_2 (555.9 μg/L) > $O_3/FeOOH$ (506.9 μg/L) > O_3/MgO (400.7 μg/L). However, with regard to $HOBr/OBr^-$, the concentration in the O_3/CeO_2 system was notably higher than that in the other systems and the order was O_3/CeO_2 (1,038.8 μg/L) > O_3 (960.4 μg/L) > $O_3/FeOOH$ (950.7 μg/L) > O_3/MgO (937.3 μg/L). In all cases, the sum of all measured bromine species (i.e. Br^-, HOBr, OBr^-, and BrO_3^-) corresponded perfectly to the initial Br^- concentration (1,800 μg/L) within 98.1 and 102.2%. The results indicate that both blocking the oxidation of Br^- to HOBr/OBr^- and the reduction of $HOBr/OBr^-$ to Br^- can be ruled out in the O_3/CeO_2 system.

Therefore, it can be deduced that the inhibition of the oxidation of $HOBr/OBr^-$ to $BrO^{\cdot}$ resulted in the BrO_3^- inhibition in O_3/CeO_2. At pH 6.3, the protonated HOBr will predominate ($pK_{a(HOBr)} = 8.9$) [11]. Moreover, the reaction between O_3 and HOBr can be neglected ($k_{OBr^-,O_3} = 100\ M^{-1}\ s^{-1}$, $k_{HOBr^-,O_3} = 0.01\ M^{-1}\ s^{-1}$), while $HO^{\cdot}$ oxidizes both HOBr and OBr^- quickly ($k_{OBr^-,HO^{\cdot}} = 4.5 \times 10^9\ M^{-1}\ s^{-1}$, $k_{HOBr^-,HO^{\cdot}} = 2 \times 10^9\ M^{-1}\ s^{-1}$). Thus, about 90% of $HOBr/OBr^-$ is estimated to be oxidized by $HO^{\cdot}$ at this pH as suggested by von Gunten et al. [11,22]. As a result, the decline of $HO^{\cdot}$ in the presence of CeO_2 during ozonation might lead to the inhibition of BrO_3^- formation.

3.2. The oxidation of pCNB during catalytic ozonation with different catalysts

pCNB, which is resistant to O_3 ($k_{pCNB,O_3} = 1.6\ M^{-1}\ s^{-1}$) but reacts quickly with $HO^{\cdot}$ ($k_{pCNB,HO^{\cdot}} = 2.6 \times 10^9\ M^{-1}\ s^{-1}$), was used to verify the speculation in Section 3.1. Primary experiments showed that the adsorption of pCNB on CeO_2 and FeOOH progressed rapidly and almost completed at the initial phase (<30 s) as depicted in Fig. 4. There was nearly no difference between CeO_2 and FeOOH with a very low adsorption amount (less than 8%).

Fig. 5 shows the time dependence of pCNB degradation in the catalytic ozonation processes. As shown in Fig. 5, the degradation of pCNB was fast during the initial phase of the catalytic ozonation and slowed down in the main phase. In single ozonation, the degradation of pCNB was relatively moderate (Fig. 5 inset). At the end of the reactions (30 min), the degradation efficiencies of pCNB by single ozonation and catalytic ozonation were in the order O_3/MgO (86.5%) > $O_3/FeOOH$ (77.6%) > O_3 (43.9%) > O_3/CeO_2 (37.9%), which was in great agreement with Ye et al. [25]. In addition, the increase in experimental temperature (from 17 to 27°C) greatly enhanced the degradation of pCNB in single ozonation, while had negligible effect in the O_3/CeO_2 process (Fig. S3, Supporting

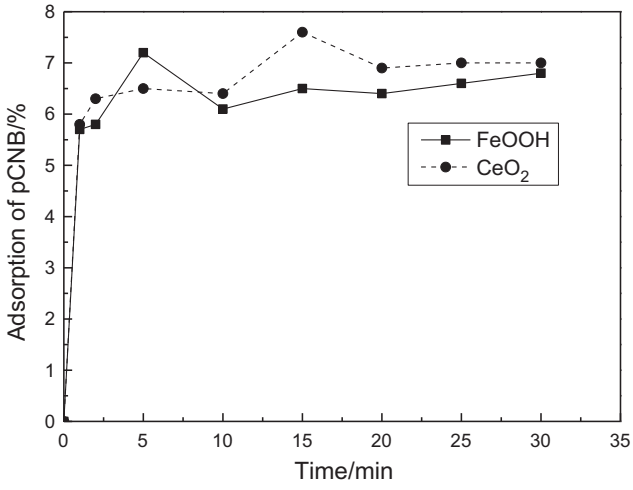

Fig. 4. The adsorption of pCNB on CeO_2 and FeOOH. $[pCNB]_0$ = 80 μg/L, catalyst dose = 100 mg/L, pH 6.3, and T = 17.4°C.

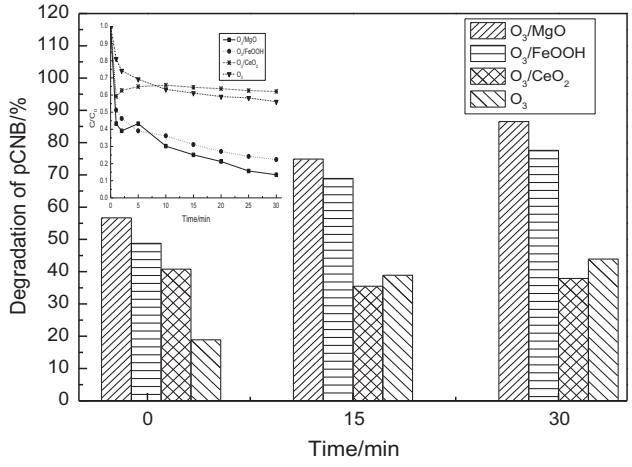

Fig. 5. Evolution of dimensionless pCNB concentration with reaction time in the ozonation and catalytic ozonation. $[O_3]_0$ = 0.40 ± 0.02 mg/L, $[pCNB]_0$ = 80 μg/L, catalyst dose = 100 mg/L, pH 6.3, and T = 17.4°C.

Information). It was noted that an abnormal break point was observed in the initial phase of the O_3/CeO_2 process (Fig. 5 inset). At this point, the removal percentage of pCNB was 40.8% and subsequently decreased to 37.3%. The measurement error was unlikely to be the cause of this abnormal result by the fact that this phenomenon was recurring in a series of studies on the O_3/CeO_2 system (data are not shown). Unfortunately, to the best of our knowledge, no explanation has yet been suggested for this phenomenon.

As is well known, the rapid degradation of pCNB in O_3/FeOOH and O_3/MgO was mainly due to the acceleration of HO• formation in solution [26,27]. In the O_3/FeOOH system, the surface hydroxyl groups will induce aqueous O_3 decomposition to generate HO•, accelerating pCNB degradation [5,26]. In the O_3/MgO system, the hydrolyzation of MgO accelerates aqueous O_3 decomposition to generate HO• in solution [27]. Similar with that in the O_3/FeOOH system, pCNB cannot complex with the surface active sites of CeO_2 in the O_3/CeO_2 system as observed in the adsorption experiments (Fig. 4), thus the degradation of pCNB was mainly ascribed to the oxidation by HO• in the bulk solution. However, the lower degradation of pCNB was obtained in O_3/CeO_2 compared with single ozonation (Fig. 5), indicating that the formation of HO• in solution was inhibited.

The presence of CeO_2 may inhibit HO• formation via two pathways: (i) scavenging of HO• by CeO_2 and (ii) hindering the route from O_3 to HO•. HO• scavenging by CeO_2 has not yet been found in the water treatment system. The species in CeO_2 for consuming HO• is likely to be Ce(III) rather than Ce(IV). However, the CeO_2 sample with more Ce(III) had lower efficiency for inhibition of BrO_3^- formation as observed in the following section. This contradictory result unambiguously ruled the pathway (i) out. Thus, the possibility of hindering the route from O_3 to HO• should be discussed.

In the bulk solution, O_3 can decompose into HO• initiated by the hydroxide ions and propagated via a series of chain reactions [1]. The reaction between ozone and hydroxide ion is the rate-limiting step of the chain reactions [28]:

$$O_3 + OH^- \rightarrow HO_2^- + O_2 \quad \left(k = 70\ M^{-1}\ s^{-1}\right) \tag{1}$$

Obviously, both O_3 and oxygen-containing species (HO_2^-, $\cdot O_2^-$, etc.) generated in the chain reactions play a significant role on HO• formation in the bulk solution. However, in the presence of CeO_2, previous researches suggested that O_3 and these oxygen-containing intermediates could be adsorbed on the active sites (i.e. Ce(III), Ce(IV), and oxygen vacancies) of CeO_2 [29–32]. Moreover, part of the adsorbed O_3 will decompose into active oxygen-containing species (e.g. superoxide, ozonide, and surface oxygen atom) rather than HO• on the catalyst surface [7,33]. Even though these active species are considered to be efficient to degrade some organic compounds such as polychlorobiphenyls, chlordanes, and hyaluronic acid, they cannot be responsible for the pCNB degradation and also the Br^- conversion due to the limited adsorption of pCNB and Br^- on the CeO_2 surface [32,34,35].

Based on the above discussion, it could be confirmed that inhibition of HO• formation in solution in

the O_3/CeO_2 system resulted in the inefficient degradation of pCNB and also the Br^- conversion. Moreover, the inhibition of HO· formation was suggested to be ascribed to the adsorption of O_3 and oxygen-containing species generated from O_3 decomposition on the CeO_2 surface. To verify this speculation, the effect of inorganic anions (i.e. NO_3^- and SO_4^{2-}) in the catalytic ozonation was investigated.

3.3. Effect of inorganic anions on BrO_3^- formation during CeO_2 catalytic ozonation

Both NO_3^- and SO_4^{2-} are the main anions in natural water. SO_4^{2-} has strong chelating ability that can notably influence the catalytic ozonation process, while NO_3^- is a relatively weaker chelator [36]. Fig. 6 shows the effect of NO_3^- and SO_4^{2-} on BrO_3^- formation during catalytic ozonation.

As shown in Fig. 6, the formation of BrO_3^- increased notably in the O_3/CeO_2 system with the addition of SO_4^{2-}, particularly when the concentration of SO_4^{2-} was less than 2 mmol/L, while the BrO_3^- formation reduced with the increase in SO_4^{2-} concentration in the O_3/FeOOH system. NO_3^- had less effect on the formation of BrO_3^- in both O_3/FeOOH and O_3/CeO_2 relative to SO_4^{2-}.

According to the previous researches, SO_4^{2-} ions will affect HO· formation via (i) HO· scavenging by SO_4^{2-} [37–39] and (ii) complexing with the catalyst surface [36]. It has been reported that hydrogen sulfate ions (HSO_4^-) generated by the reaction of SO_4^{2-} with hydrogen ions will react with HO· by the following steps [38,39]:

$$SO_4^{2-} + H^+ \leftrightarrow HSO_4^- \quad (2)$$

$$HSO_4^- + HO\cdot \rightarrow SO_4^{\cdot-} + H_2O \quad \left(k = 1.4 \times 10^7\ M^{-1}\,s^{-1}\right) \quad (3)$$

As seen from Eq. (2), the dissociation equilibrium exists between SO_4^{2-} and HSO_4^-. Taking the SO_4^{2-} concentration (≤10 mM) into account, the formed HSO_4^- (ca. 0.49 μM, see Text. S2 for detailed calculation, Supporting Information) is negligible relative to Br^- (13.75 μM). In addition, the rate constant of Eq. (3) is two orders of magnitude lower than that of reactions between HO· and Br species (i.e. Br^- and HOBr/OBr^-) as shown in Fig. 3. Therefore, the possibility of HO· scavenging by SO_4^{2-} can be unambiguously ruled out, which is in consistent with Zhu et al. [37].

Since SO_4^{2-} ions have strong affinity to the metal oxides as reported elsewhere [36], the adsorption of SO_4^{2-} on FeOOH and CeO_2 in water was examined in the present study and the result is shown in Fig. 7. It was found that an extremely rapid adsorption of SO_4^{2-} on CeO_2 occurred within 0.5 min and nearly completed after 5 min (Fig. 7). After 30 min, about 55% of SO_4^{2-} (5.5 μM) was adsorbed on the CeO_2 surface; on the contrary, a much smaller amount of SO_4^{2-} (1.2 μM) was adsorbed on FeOOH.

In the case of O_3/FeOOH, it has been reported that the outer-sphere surface complexes with SO_4^{2-} will be formed on the surface of FeOOH and meanwhile, ligand exchange with some surface hydroxyl groups

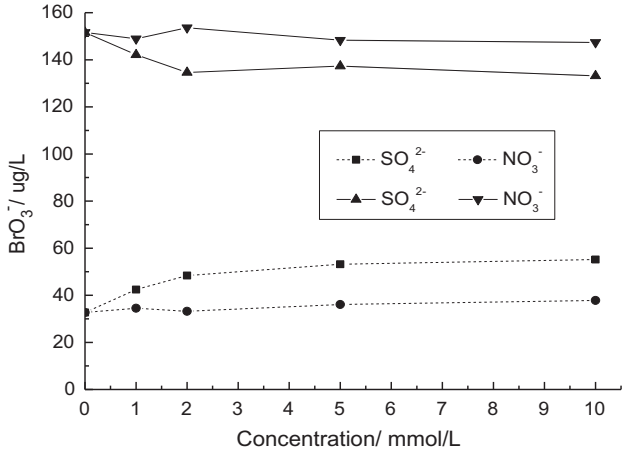

Fig. 6. Effect of sulfate and nitrate on the controlling of bromate formation during catalytic ozonation in the presence of CeO_2 and FeOOH. The solid lines: O_3/FeOOH; the dashed lines: O_3/CeO_2 $[Br^-]_0$ = 1.1 mg/L, $[O_3]_0$ = 5.21 mg/L, catalyst dose = 100 mg/L, T = 18 ℃, pH 6.30, and reaction time = 30 min.

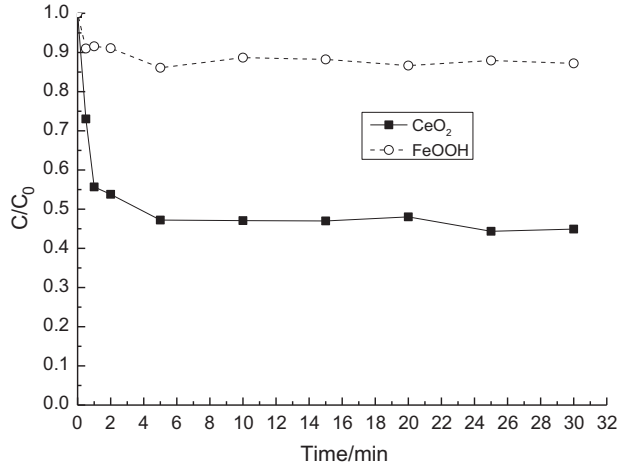

Fig. 7. Adsorption of sulfate on CeO_2 and FeOOH. Catalyst dose = 100 mg/L, T = 18 ℃, pH 6.30, and $[SO_4^{2-}]_0$ = 10 μM.

by SO_4^{2-} ions will occur [36]. The surface hydroxyl groups directly relate to the activity of catalyst to promote the generation of HO· [26]. Therefore, it can be concluded that the addition of SO_4^{2-} decreased the amount of active hydroxyl groups and then inhibited the HO· formation which resulted in the reduction of BrO_3^- formation in the O_3/FeOOH system. In the O_3/CeO_2 system, the SO_4^{2-} ions competed the surface Ce(IV) sites [40], resulting in the less adsorption of O_3 and oxygen-containing species on the catalyst surface and then weakened the inhibitory effect of BrO_3^- formation (Fig. 6) [33,41].

Combined with the discussion in Section 3.2, it can be demonstrated that the adsorption of O_3 and oxygen-containing species on the CeO_2 surface directly inhibits the BrO_3^- formation. To better understand the inhibition mechanism of BrO_3^- in the O_3/CeO_2 system, the physical properties (e.g. structure, composition, and crystallite size) of CeO_2 which directly relate to the adsorption process should be further explored. Thus, the effect of calcination temperature of the CeO_2 samples on the BrO_3^- formation was investigated.

3.4. Effect of calcination temperature on the formation of bromate in catalytic ozonation

Normally, calcination is the primary factor causing microscopic changes in the crystallite size of a sample. With increasing calcination temperature, a series of changes (such as decomposition and dehydration) will occur, ultimately causing aggregation or the formation of new particles [42]. Thus, the BrO_3^- formation and also the Br mass balance during catalytic ozonation by CeO_2 calcined at different temperatures were investigated and the results are shown in Fig. 8.

Fig. 8(a) shows that the CeO_2 samples calcined at different temperatures had varying abilities to limit the formation of BrO_3^- during catalytic ozonation. Obviously, CeO_2 (450˚C) showed the greatest efficiency to control the BrO_3^- formation during ozonation and the ability of these CeO_2 samples to control BrO_3^- formation follows the trend CeO_2 (450˚C) > CeO_2 (650˚C) > CeO_2 (250˚C). The mass balance of Br depicted in Fig. 8(b) showed that in all cases, the sum of measured bromine species (i.e. Br^-, HOBr, OBr^-, and BrO_3^-) corresponded perfectly to the initial bromide concentration (1,100 μg/L) within 98.6 and 101.9%. In addition, the highest concentration of $HOBr/OBr^-$ (517.7 μg/L) was observed in the catalytic ozonation with CeO_2 (450˚C) at 30 min (Fig. 8(b)).

Generally, the calcined CeO_2 contains Ce(IV), Ce(III), and also a certain number of lattice defects [43]. After calcination at different temperatures, there are a lot of differences in the crystallite size, specific surface area, the concentration of Ce(IV) and Ce(III), and also the amount of lattice defects among the CeO_2 samples [42]. Thus, XRD and XPS analyses on CeO_2 calcined at different temperatures were carried

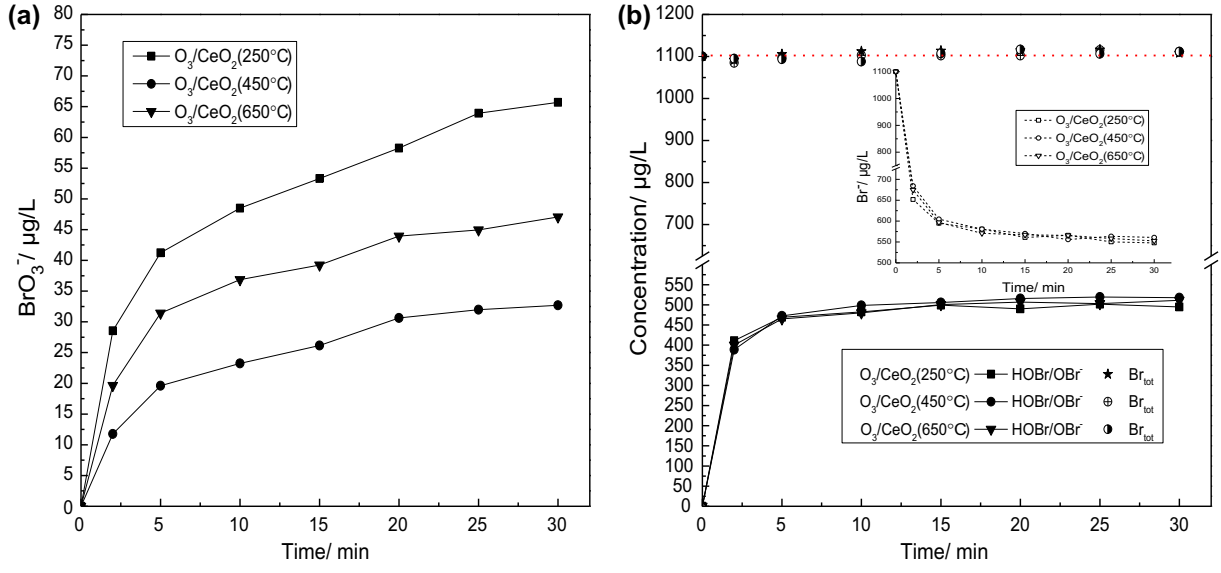

Fig. 8. (a) The bromate formation during catalytic ozonation with CeO_2 calcined at different temperatures and (b) concentration profiles of Br^- and $HOBr/OBr^-$ and the corresponding total bromine mass balance during CeO_2 catalytic ozonation. Br_{tot}: sum of all bromine species (i.e. Br^-, HOBr, OBr^-, and BrO_3^-). $[Br^-]_0$ = 1.1 mg/L, $[O_3]_0$ = 5.21 mg/L, catalyst dose = 100 mg/L, T = 18˚C, and pH 6.30.

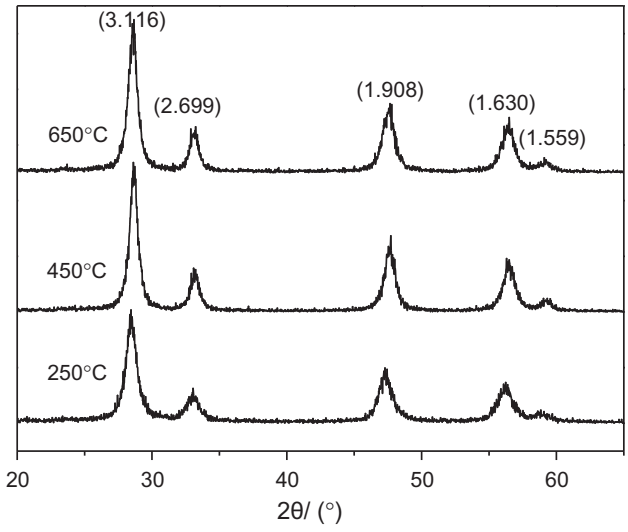

Fig. 9. XRD patterns of samples calcined at different temperatures.

out to investigate the main factors influencing the inhibitory effect of CeO_2 on BrO_3^- formation during ozonation. The XRD patterns of CeO_2 samples calcined at different temperatures are summarized in Fig. 9.

As can be seen from Fig. 9, the diffraction peaks appeared at $2\theta = 28.66$, 33.16, 47.64, and 56.40 in all samples, with d-values of 3.116, 2.699, 1.908, and 1.630 corresponding to the (1 1 1), (2 0 0), (2 2 0), and (3 1 1) crystal faces of CeO_2, respectively. The d-values of the diffraction peaks of the samples tested are in consistent with those presented on the pattern of a standard CeO_2 sample (JCPDS4-0593), indicating that all of the CeO_2 samples are pure with an intact cubic fluorite structure.

The X-ray diffraction peak of the sample calcined at 250˚C was relatively less intense than the others, and the full width at half maximum (FWHM) was wider. FWHM can be used to determine the crystallite size by the Scherrer equation [44]:

$$D = K\lambda/B_{1/2}\cos\theta \quad (4)$$

where K—Scherrer constant, $K = 0.89$; D—Crystallite size/(nm); $B_{1/2}$—FWHM/(rad); θ—diffraction angle/(rad) and λ—wavelength of diffraction lines/(nm), $\lambda = 0.154056$ nm.

The results are summarized in Table 1. Combined with Fig. 9 and Table 1, it is found that the CeO_2 sample calcined at 250˚C had a good crystal shape and the corresponding crystallite size was the smallest compared with the other samples. The first sharp diffraction peak (FSDP) appeared in the sample calcined at 450˚C, and the peak width became narrower, indicating an increase in the crystallite size. The characteristics of the XRD pattern of the sample calcined at 650˚C were similar to those found for the sample calcined at 450˚C. The level of crystallinity increased as the calcination temperature increased. However, the degree of lattice agglomeration also increased, and the specific surface area of the sample diminished as shown in Table 1. Visually, this was observed as a gradual change in the color of CeO_2 from yellow to yellow-white. This might be due to the fact that the adsorption of light by smaller particles is stronger than by the larger particles [45].

The above results indicate that neither the crystallite size nor the specific surface area of the CeO_2 samples is related to the performance of BrO_3^- limitation during CeO_2 catalytic ozonation. Thus, XPS analysis on CeO_2 samples subjected to different calcination temperatures was carried out. The results were fitted with O_{1S}, Ce curves as shown in Figs. 10 and 11, respectively.

Fig. 10 shows O_{1S} curves of the CeO_2 samples obtained after calcination for 2 h at temperatures of 250, 450, and 650˚C. The two peaks obtained after fitting represent adsorbed oxygen and lattice oxygen [46]. The high-binding energy peak corresponds to adsorbed oxygen, while the lower one corresponds to lattice oxygen. The adsorbed oxygen on the surface of CeO_2 always presents in the form of both O_2 and O_2^-. The relative proportions of lattice oxygen and adsorbed oxygen after fitting are summarized in Table 2.

As shown in Table 2, the peak areas of both lattice oxygen and adsorbed oxygen for the CeO_2 sample

Table 1
Major characteristics of the CeO_2 samples calcined at different temperatures

Catalyst	Diffraction angle (rad)	FWHM (rad)	Crystallite size (nm)[a]	BET specific surface area ($m^2\ g^{-1}$)
CeO_2 (250˚C)	0.49601	0.01267	11.162	164.3
CeO_2 (450˚C)	0.50019	0.01121	12.629	116.8
CeO_2 (650˚C)	0.49916	0.01063	13.311	73.1

[a]XRD determined.

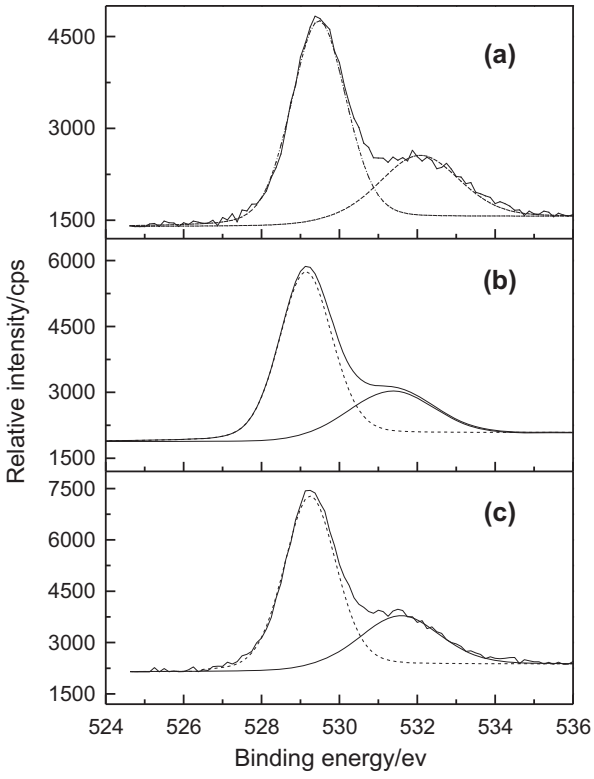

Fig. 10. O_{1s} XPS spectra for CeO_2 samples calcined at different temperatures (a) CeO_2 calcined at 250℃, (b) CeO_2 calcined at 450℃, and (c) CeO_2 calcined at 650℃.

calcined at 450℃ were much smaller than those observed for CeO_2 calcined at 250℃ and 650℃. The peak areas of lattice oxygen and adsorbed oxygen decreased in the order CeO_2 (250℃) > CeO_2 (650℃) > CeO_2 (450℃), a trend that was diametrically opposed to the ability of each catalyst to control the BrO_3^- formation (Fig. 8(a)). The result indicates that less lattice oxygen and adsorbed oxygen have a positive effect on the BrO_3^- inhibition.

Fig. 11 shows Ce-fitted curves of the CeO_2 samples exposed to different calcination temperatures. Taking the effect of spin–orbit splitting into account, there are 10 fitted peaks, half of which are v-series peaks and the remaining are u-series peaks. Trivalent Ce(III) is designated as a 4-peak structure with its v_0 and v_1 peaks appearing at 880.1 and 885.2 eV, a sign of the existence of Ce(III). Spin–orbit splitting u_0 and u_1 peaks that corresponded to v_0 and v_1 appear at 901.2 and 904.8 eV, respectively. Analogously, tetravalent Ce (IV) showed a 6-peak structure, and its u, u_2, and u_3 peaks are located at 882.1, 888.3, and 898.2 eV, respectively. The corresponding spin–orbit splitting u, u_2, and u_3 peaks appear at 900.4, 907.3, and 916.3 eV [47].

The peak areas located at different binding energy and proportions are shown in Table 3. The proportion of Ce(III) in CeO_2 is calculated using the following formula [48]:

$$C(\mathrm{Ce(III)}) = (v_0 + v_1 + \mu_0 + \mu_1)/\sum_i (\mu_i + v_i) \quad (5)$$

After calculation, the proportions of Ce(III) in the CeO_2 samples calcined at 250, 450, and 650℃ are found to be 20.25, 12.88, and 18.48%, respectively, while the proportions of Ce(IV) are found as 79.75 , 87.12, and 81.52%.

The proportion of Ce(III) decreases in the order CeO_2 (250℃) > CeO_2 (650℃) > CeO_2 (450℃), whereas for Ce(IV), the order is CeO_2 (450℃) > CeO_2 (650℃) > CeO_2 (250℃). This is similar to the trend in the ability of the different CeO_2 samples to control the BrO_3^- formation as shown in Fig. 8(a). The result indicates that a larger amount of Ce(IV) relative to Ce(III) on the CeO_2 surface has a positive effect on the BrO_3^- inhibition. Surface Ce(IV) species are the main active sites for O_3 and oxygen-containing species adsorption [33]. Thus, the presence of more Ce(IV) leads to more efficient inhibition of HO· formation. Moreover, the less lattice oxygen and adsorbed oxygen lead to the appearance of more oxygen vacancies and a greater oxygen storage capacity, promoting the adsorption of oxygen-containing species on the CeO_2 surface and then the inhibition of HO· formation is enhanced.

3.5. The BrO_3^- inhibition mechanism in the O_3/CeO_2 system

From the above discussion, it could be concluded that the BrO_3^- inhibition in the O_3/CeO_2 system is mainly ascribed to the inhibition of HO· formation in solution. The inhibition of HO· formation is caused by the adsorption of O_3 and oxygen-containing intermediates, which is directly depended on the active sites on the CeO_2 surface.

Bulanin et al. [33] suggested that O_3 molecules in gaseous phase can be adsorbed on the CeO_2 surface via various ways (e.g. adsorption on Ce(IV) and Ce(III) sites, interaction with Lewis basic sites, and a weak H–bond with surface hydroxyl groups). In aqueous phase with the presence of H_2O, though it remains confused that whether the same process occurs, it has been commonly accepted that O_3 molecules can be adsorbed on Ce(IV) sites via one of the terminal oxygen atoms to yield some active species on the surface [7]. These active species on the CeO_2

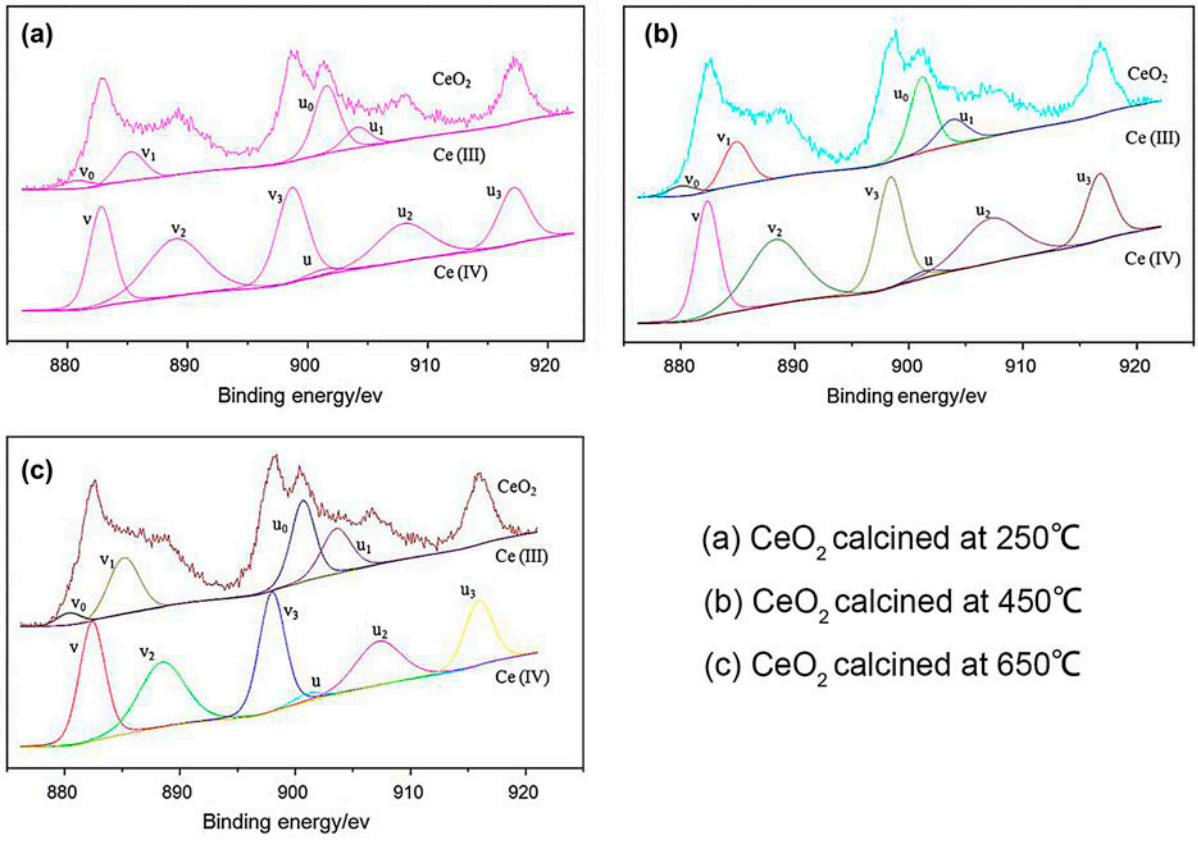

Fig. 11. Ce XPS spectra for CeO_2 samples calcined at different temperatures.

Table 2
The peak area of the samples (Ce) calcined at different temperatures under the conditions of the binding energy

	250℃		450℃		650℃	
Binding energy/eV	Peak area	Proportion (%)	Peak area	Proportion (%)	Peak area	Proportion (%)
532.06 (adsorbed oxygen)	2,904	31.16	1,775	27.41	2,741	30.73
529.47 (lattice oxygen)	6,416	68.84	4,701	72.59	6,180	69.27

surface cannot be responsible for the Br^- conversion in solution because Br^- ions cannot be adsorbed on the surface of catalyst. Further experimental results confirmed that the adsorption of O_3 on Ce(IV) sites can be poisoned by the addition of SO_4^{2-}, resulting in the weakened inhibition of BrO_3^- formation (Fig. 6). Moreover, the CeO_2 sample calcined at 450℃, which possesses the most Ce(IV) sites, has the best inhibitory effect on the BrO_3^- formation (Fig. 8(a)).

In addition, as is reported, the CeO_2 samples lack oxygen after calcination, which will lead to the formation of a continuum of O-deficient non-stoichiometric compositions of the type CeO_{2-x} [30,43]. The oxygen defect vacancies will be refilled upon exposure of CeO_{2-x} to the oxygen-enriched environment, giving CeO_2 a high "oxygen storage capacity" [43]. Thus, the appearance of more oxygen vacancies (i.e. less lattice oxygen) will be able to adsorb more oxygen-containing species. The experimental results show obviously that the CeO_2 sample calcined at 450℃ which has the least lattice oxygen inhibits the BrO_3^- formation most effectively. In addition, the less adsorbed oxygen on the CeO_2 surface also enhances the adsorption of oxygen-containing species. Furthermore, as suggested by the previous researches [41,43,49], both Ce(IV) and Ce (III) sites could adsorb oxygen-containing species in the bulk solution via various ways.

It should be noted that CeO_2 catalytic ozonation inhibited the BrO_3^- formation as observed in the present study. In contrast, the BrO_3^- formation was

Table 3
The peak area of the samples (Ce) calcined at different temperatures under the conditions of the binding energy

	250℃		450℃		650℃	
Binding energy/eV	Peak area	Proportion (%)	Peak area	Proportion (%)	Peak area	Proportion (%)
880.10	433	1.34	329	1.41	462	1.45
882.33	4,977	15.44	3,542	15.21	5,351	16.79
885.4	1,486	4.61	1,375	5.9	2,713	8.51
888.30	6,734	20.89	4,651	19.97	5,219	16.37
898.50	5,954	18.47	3,951	16.96	5,359	16.81
901.17	396	1.23	2,413	10.36	3,373	10.58
901.50	3,535	10.97	285	1.22	398	1.25
904.15	1,075	3.33	1,014	4.35	2,317	7.27
907.18	4,136	12.83	3,377	14.5	3,511	11.01
916.75	3,510	10.89	2,357	10.12	3,175	9.96

promoted during catalytic ozonation with MgO and FeOOH compared with single ozonation. This discrepancy is mainly ascribed to the different mechanisms for HO· formation in solution. The HO· formation is accelerated in O_3/MgO and O_3/FeOOH, while it is inhibited to some extent in the CeO_2 catalytic ozonation.

4. Conclusions

In the present study, CeO_2 catalytic ozonation showed a great efficiency of BrO_3^- inhibition compared with single ozonation and catalytic ozonation with MgO and FeOOH. To further realize the BrO_3^- inhibition mechanism, the degradation of pCNB, the effect of inorganic anions and calcination temperature, XRD, and also XPS analysis are conducted.

(1) The lower degradation of pCNB in the O_3/CeO_2 system confirmed that the inhibition of HO· formation resulted in the BrO_3^- inhibition. However, in both O_3/FeOOH and O_3/MgO, the O_3 decomposition was accelerated to promote HO· formation in the bulk solution.
(2) The addition of SO_4^{2-} weakened the inhibition of BrO_3^- formation significantly in O_3/CeO_2 through competing the active sites of CeO_2, indicating that the adsorption of O_3 molecules and also oxygen-containing species in solution on the CeO_2 surface led to the inhibition of BrO_3^- formation.
(3) The BrO_3^- formation was strongly inhibited in the catalytic ozonation with CeO_2 calcined at 450℃. XPS analysis on the CeO_2 samples confirmed that the presence of more Ce(IV) sites provided more active sites for O_3 and oxygen-containing species adsorption; the less lattice oxygen and adsorbed oxygen resulted in the appearance of more oxygen vacancies and a greater oxygen storage capacity of CeO_2, enhancing the adsorption of oxygen-containing species and O_3 molecules in solution.

To sum up, the inhibition of BrO_3^- formation in the O_3/CeO_2 system arises from the inhibition of HO· formation in solution as a result of the adsorption of O_3 and oxygen-containing species on the CeO_2 surface.

Supplementary material

The supplementary material for this paper is available online at http://dx.doi 10.1080/19443994.2015.1079261.

Acknowledgments

This research was supported by Major Science and Technology Program for Water Pollution Control and Treatment (2009ZX07424-005-02). We gratefully acknowledge anonymous reviewers for the valuable comments and constructive suggestions and both Dr Yongze Liu and Dr Congwei Luo for fruitful discussion.

References

[1] U. von Gunten, Ozonation of drinking water: Part I. oxidation kinetics and product formation, Water Res. 37(2003) 1443–1467.
[2] J. Nawrocki, B.K. Hordern, The efficiency and mechanisms of catalytic ozonation, Appl. Catal., B 99 (2010) 27–42.

[3] S.D. Richardson, T.A. Ternes, Water analysis: Emerging contaminants and current issues, Anal. Chem. 83 (2011) 4614–4648.
[4] F. Qi, B. Xu, Z. Chen, L. Feng, L. Zhang, D. Sun, Catalytic ozonation of 2-isopropyl-3-methoxypyrazine in water by γ-AlOOH and γ-Al_2O_3: Comparison of removal efficiency and mechanism, Chem. Eng. J. 219 (2013) 527–536.
[5] T. Zhang, J. Ma, Catalytic ozonation of trace nitrobenzene in water with synthetic goethite, J. Mol. Catal. A: Chem. 279 (2008) 82–89.
[6] F.J. Beltrán, F.J. Rivas, R.M. de Espinosa, A TiO_2/Al_2O_3 catalyst to improve the ozonation of oxalic acid in water, Appl. Catal., B 47 (2004) 101–109.
[7] R. Rosal, A. Rodríguez, M.S. Gonzalo, E.G. Calvo, Catalytic ozonation of naproxen and carbamazepine on titanium dioxide, Appl. Catal., B 84 (2008) 48–57.
[8] Y. Kurokawa, Y. Hayashi, A. Maekawa, M. Takahashi, S. Odashima, Carcinogenicity of potassium bromate administered orally to F334 rats, J. Natl. Cancer Inst. 71 (1983) 965–972.
[9] T.P. Bonacquisti, A drinking water utility's perspective on bromide, bromate, and ozonation, Toxicology 221 (2006) 145–148.
[10] U. von Gunten, Y. Oliveras, Advanced oxidation of bromide-containing waters: Bromate formation mechanisms, Environ. Sci. Technol. 32 (1998) 63–70.
[11] U. Pinkernell, U. von Gunten, Bromate minimization during ozonation: Mechanistic considerations, Environ. Sci. Technol. 35 (2001) 2525–2531.
[12] M.O. Buffle, S. Galli, U. von Gunten, Enhanced bromate control during ozonation: The chlorine-ammonia process, Environ. Sci. Technol. 38 (2004) 5187–5195.
[13] Y.L. Nie, C. Hu, L. Yang, J.C. Hu, Inhibition mechanism of BrO_3^- formation over MnOx/Al2O3 during the catalytic ozonation of 2,4-dichlorophenoxyacetic acid in water, Sep. Purif. Technol. 117 (2013) 41–45.
[14] Y.L. Nie, C. Hu, N.N. Li, L. Yang, J.H. Qu, Inhibition of bromate formation by surface reduction in catalytic ozonation of organic pollutants over β-FeOOH/Al_2O_3, Appl. Catal., B 147 (2014) 287–292.
[15] H.W. Yang, S.X. Yang, L. Wu, W.J. L, $Ce_xZr_{1-x}O_2$ mixed oxides applied to minimize the bromate formation in the catalytic ozonation of a filtered water, Catal. Commun. 15 (2011) 99–102.
[16] T. Zhang, W.P. Chen, J. Ma, Z. Qiang, Minimizing bromate formation with cerium dioxide during ozonation of bromide-containing water, Water Res. 42 (2008a) 3651–3658.
[17] K. Kandori, M. Fukuoka, T. Ishikawa, Effects of citrate ions on the formation of ferric oxide hydroxide particles, J. Mater. Sci. 26 (1991) 3313–3319.
[18] S. Morales, R. Cela, Highly selective and efficient determination of US environmental protection agency priority phenols employing solid-phase extraction and non-aqueous capillary electrophoresis, J. Chromatogr. A 896 (2000) 95–104.
[19] R. Cousin, E.A. Aad, S. Capelle, D. Courcot, J.F. Lamonier, A. Aboukaïs, Physico-chemical study of impregnated Cu and V species on CeO2 support by thermal analysis, XRD, EPR, 51V-MAS-NMR and XPS, J. Mater. Sci. 42 (2007) 6188–6196.
[20] T. Zhang, P. Hou, Z.M. Qiang, X.W. Lu, Q.H. Wang, Reducing bromate formation with H^+-form high silica zeolites during ozonation of bromide-containing water: Effectiveness and mechanisms, Chemosphere 82 (2011) 608–612.
[21] U. von Gunten, J. Hoigne, Bromate formation during ozonation of bromide-containing waters: Interaction of ozone and hydroxyl radical reactions, Environ. Sci. Technol. 28 (1994) 1234–1242.
[22] U. von Gunten, Ozonation of drinking water: Part II. Disinfection and by-product formation in presence of bromide, iodide or chlorine, Water. Res. 37(2003) 1469–1487.
[23] K. Ozekin, P. Westerhoff, G. Amy, M. Siddiqui, Molecular ozone and radical pathways of bromate formation during ozonation, J. Environ. Eng-ASCE 124 (1998) 456–462.
[24] W.R. Haag, J. Hoigne, Ozonation of bromide-containing waters: Kinetics of formation of hypobromous acid and bromate, Environ. Sci. Technol. 17 (1983) 261–267.
[25] M.M. Ye, Z.L. Chen, J.M. Shen, Y. Ben, Z.Z. Xu, Synthesis of lanthanum oxide and cerium oxide and ozonation catalytic activities of *p*-chloronitrobenzene, J. Harbin Inst. Tech. 41 (2009) 77–80.
[26] T. Zhang, C.J. Li, J. Ma, H. Tian, Z.M. Qiang, Surface hydroxyl groups of synthetic α-FeOOH in promoting OH generation from aqueous ozone: Property and activity relationship, Appl. Catal., B 82 (2008b) 131–137.
[27] K. He, Y.M. Dong, Z. Li, L. Yin, A.M. Zhang, Y.C. Zheng, Catalytic ozonation of phenol in water with natural brucite and magnesia, J. Hazard. Mater. 159 (2008) 587–592.
[28] J. Staehelin, J. Hoigne, Decomposition of ozone in water: Rate of initiation by hydroxide ions and hydrogen peroxide, Environ. Sci. Technol. 16 (1982) 676–681.
[29] K.M. Bulanin, J.C. Lavalley, A.A. Tsyganenko, IR spectra of adsorbed ozone, Colloids Surf., A 101 (1995) 153–158.
[30] A. Trovarelli, Structural and oxygen storage/release properties of CeO_2-based solid solutions, Comments Inorg. Chem. 20 (1999) 263–284.
[31] M.F. Pinheiro da Silva, L.S. Soeira, K.R.P. Daghastanli, T.S. Martins, I.M. Cuccovia, R.S. Freire, P.C. Isolani, CeO_2-catalyzed ozonation of phenol: The role of cerium citrate as precursor of CeO_2, J. Therm. Anal. Calorim. 102 (2010) 907–913.
[32] W.W. Li, Z.M. Qiang, T. Zhang, F.L. Cao, Kinetics and mechanism of pyruvic acid degradation by ozone in the presence of PdO/CeO_2, Appl. Catal., B 113–114 (2012) 290–295.
[33] K.M. Bulanin, J.C. Lavalley, J. Lamotte, L. Mariey, N.M. Tsyganenko, A.A. Tsyganenko, Infrared study of ozone adsorption on CeO_2, J. Phys. Chem. B 102 (1998) 6809–6816.
[34] K. Matsunaga, M. Imanaka, K. Kenmotsu, J. Oda, S. Hino, M. Kadota, H. Fujiwara, T. Mori, Superoxide radical-induced degradation of polychlorlbiphenyls and chlordanes at low temperature, Bull. Environ. Contam. Toxicol. 46 (1991) 292–299.
[35] S.F. Wong, B. Halliwell, R. Richmond, W.R. Skowroneck, The role of superoxide and hydroxyl radicals in the degradation of hyaluronic acid induced by metal ions and by ascorbic acid, J. Inorg. Biochem. 14 (1981) 127–134.

[36] D. Peak, R.G. Ford, D.L. Sparks, An *in situ* ATR-FTIR investigation of sulfate bonding mechanisms on goethite, J. Colloid Interface Sci. 218 (1999) 289–299.
[37] X.D. Zhu, M.A. Nanny, E.C. Butler, Effect of inorganic anions on the titanium dioxide-based photocatalytic oxidation of aqueous ammonia and nitrite, J. Photochem. Photobiol., A 185 (2007) 289–294.
[38] P. Neta, R.R. Huie, A.B. Ross, Rate constants for reactions of inorganic radicals in aqueous solution, J. Phys. Chem. Ref. Data 17 (1988) 1027–1262.
[39] J.D. Laat, G. Truong Le, B. Legube, A comparative study of the effects of chloride, sulfate and nitrate ions on the rates of decomposition of H_2O_2 and organic compounds by Fe(II)/H_2O_2 and Fe(III)/H_2O_2, Chemosphere 55 (2004) 715–723.
[40] J.Z. Gao, Y.L. Qi, W. Yang, X.J. Guo, S.Y. Li, X.E. Li, Shape control of CeO_2 nano-particles and synthesis of nano-metric solid acid SO_4^{2-}/CeO_2, Mater. Chem. Phys. 82 (2003) 602–607.
[41] Y.M. Choi, H. Abernathy, H.T. Chen, M.C. Lin, M. Liu, Characterization of O_2-CeO_2 interactions using *in situ* Raman spectroscopy and first-principle calculations, Chemphyschem 7 (2006) 2006.
[42] M. Waqif, P. Bazin, O. Saur, J.C. Lavalley, G. Blanchard, O. Touret, Study of ceria sulfation, Appl. Catal., B 11 (1997) 193–205.
[43] C.T. Campbell, C.H.F. Peden, Chemistry: Oxygen vacancies and catalysis on ceria surfaces, Science 309 (2005) 713–714.
[44] A.T. D'Agostino, Determination of thin metal film thickness by X-ray diffractometry using the Scherrer equation, atomic absorption analysis and transmission/reflection visible spectroscopy, Anal. Chim. Acta 262 (1992) 269–275.
[45] X.C. Li, R.Z. Gong, Z.K. Feng, J.B. Yan, X. Shen, H.H. He, Effect of particle size and concentration on microwave-absorbing properties of $CuxCo_{2-x}Y$ (x = 0, 1) hexaferrite composites, J. Am. Ceram. Soc. 89 (2006) 1450–1452.
[46] A. Bielanski, J. Haber, Oxygen in Catalysis, Mareel Dekker Inc, New York, NY, 1991.
[47] Y. Mei, J.P. Yan, Z.R. Nie, XPS study on the influence of calcination conditions to cerium ion valence, Spectrosc. Spect. Anal. 30 (2010) 270–273.
[48] A. Pfau, K.D. Schierbaum, The electronic structure of stoichiometric and reduced CeO_2 surfaces: An XPS, UPS and HREELS study, Surf. Sci. 321 (1994) 71–80.
[49] H.T. Chen, J.G. Chang, H.L. Chen, S.P. Ju, Identifying the O_2 diffusion and reduction mechanisms on CeO_2 electrolyte in solid oxide fuel cells: A DFT + U study, J. Comput. Chem. 30 (2009) 2433–2442.